

M. MOSIALEK^{*,**}, M. DUDEK^{***}, J. WOJEWODA-BUDKA^{****}

COMPOSITE $\text{La}_{0.6}\text{Sr}_{0.4}\text{Co}_{0.8}\text{Fe}_{0.2}\text{O}_3/\text{Ag}$ CATHODE FOR SOFCs WITH $\text{Ce}_{0.8}\text{Sm}_{0.2}\text{O}_{1.9}$ ELECTROLYTE

KOMPOZYTOWA KATODA $\text{La}_{0.6}\text{Sr}_{0.4}\text{Co}_{0.8}\text{Fe}_{0.2}\text{O}_3/\text{Ag}$ DO STAŁO-TLENKOWYCH OGNIW PALIWOWYCH Z ELEKTROLITEM $\text{Ce}_{0.8}\text{Sm}_{0.2}\text{O}_{1.9}$

Influence of the short time external polarization of silver electrode contacted $\text{Ce}_{0.8}\text{Sm}_{0.2}\text{O}_{1.9}$ electrolyte was studied. Silver is moving along the $\text{Ce}_{0.8}\text{Sm}_{0.2}\text{O}_{1.9}$ surface during the -0.5 V cathodic polarization at 600°C. It caused both the increase of the electrode – electrolyte contact area and the triple phase boundary length but also decrease of electrolyte and polarization resistances. Deposit of silver oxide was found at the place where the electrode polarized at the potential of 0.5 V contacted the electrolyte and around. The decrease of electrolyte and polarization resistance was smaller but more stable in this case. Composite cathodes were obtained on $\text{Ce}_{0.8}\text{Sm}_{0.2}\text{O}_{1.9}$ electrolyte with the double step sintering procedure. Silver introduced into a $\text{La}_{0.6}\text{Sr}_{0.4}\text{Co}_{0.8}\text{Fe}_{0.2}\text{O}_3$ cathode improved a performance of a $\text{La}_{0.6}\text{Sr}_{0.4}\text{Co}_{0.8}\text{Fe}_{0.2}\text{O}_3|\text{Ce}_{0.8}\text{Sm}_{0.2}\text{O}_{1.9}|\text{Ni}$ cell by 33%.

Keywords: SOFC, cathode, LSCF, silver, SDC

Zbadano wpływ zewnętrznej polaryzacji na elektrodę srebrną w kontakcie z elektrolitem tlenkowym $\text{Ce}_{0.8}\text{Sm}_{0.2}\text{O}_{1.9}$. W czasie polaryzacji katodowej przy potencjale elektrody równym -0.5 V w temperaturze 600°C srebro migruje po powierzchni elektrolitu. Powoduje to zarówno wzrost powierzchni kontaktu elektrody z elektrolitem jak i długości linii styku trzech faz. Powoduje to również spadek rezystancji elektrolitu oraz rezystancji polaryzacyjnej. W miejscu styku elektrody polaryzowanej potencjałem 0,5 V i elektrolitu oraz w jego pobliżu stwierdzono obecność tlenku srebra. Spadek rezystancji elektrolitu i rezystancji polaryzacyjnej był w tym przypadku mniejszy ale bardziej stabilny. Wykonano kompozytowe katody $\text{Ag}/\text{La}_{0.6}\text{Sr}_{0.4}\text{Co}_{0.8}\text{Fe}_{0.2}\text{O}_3$ metodą dwustopniowego spiekania na podłożu elektrolitu $\text{Ce}_{0.8}\text{Sm}_{0.2}\text{O}_{1.9}$. Wprowadzenie srebra do struktury katody $\text{La}_{0.6}\text{Sr}_{0.4}\text{Co}_{0.8}\text{Fe}_{0.2}\text{O}_3$ podniosło moc ogniwa $\text{La}_{0.6}\text{Sr}_{0.4}\text{Co}_{0.8}\text{Fe}_{0.2}\text{O}_3|\text{Ce}_{0.8}\text{Sm}_{0.2}\text{O}_{1.9}|\text{Ni}$ o 33%.

1. Introduction

Nowadays the solid oxide fuel cells (SOFCs) research concentrates on the intermediate temperature (IT) region of interest. Many novel electrode and electrolyte materials were reported so far. Among others silver does not attract researchers attention as promising cathode material. Silver is the best electronic conductor, it is ductile and cheap. Baker et al [1] compared several noble metals and perovskite cathode materials using point electrodes. They stated that silver exhibits excellent electrocatalytic properties for the oxygen reduction reaction (ORR). Jiménez et al [2] examined Aglyttria stabilized zirconia (YSZ) half-cell. They described the impact of oxygen solubility in metallic silver on ORR, founding that ORR occurs not only at the triple phase boundary (tpb) but also at the surface between silver and an electrolyte due to the presence of dissolved oxygen. Silver reveal some disadvantages such as the low melting point of 961°C, high volatility and electromigration in the electric field [3-5]. Last two be-

comes less and less important at lower temperatures. Silver is often used as sealant or current collector. Several attempts to use silver as a cathode material were described. It was used in the composite cathode materials with electrolyte [6-9] and with other cathode material [10-19].

$\text{La}_{0.6}\text{Sr}_{0.4}\text{Co}_{0.8}\text{Fe}_{0.2}\text{O}_3$ (LSCF) reveal very good catalytic activity in ORR and conducts ionic current both at surface and by the bulk [20]. It reveals the thermal expansion coefficient similar to ceria based electrolytes, and has higher ionic conductivity than most perovskites [21].

Ceria based electrolytes reveal better ionic conductivities than typically used YSZ in IT temperature range. Samaria doped ceria (SDC), gadolinia doped ceria (GDC) and two cations doped ceria are mostly used promising ceria electrolyte materials [22-24]. These electrolytes do not react with cathode materials containing cobalt resulting in insulate phase appearing.

Dusastre and Kilner [21] showed that LSCF cathode performance can be improved by addition of 36% by volume of

* INSTITUTE OF CATALYSIS AND SURFACE CHEMISTRY PAS, 30-239 CRACOW, POLAND

** INSTITUTE OF PHYSICAL CHEMISTRY PAS, WARSAW, POLAND

*** AGH –UNIVERSITY OF SCIENCE AND TECHNOLOGY, FACULTY OF FUELS AND ENERGY, CRACOW, POLAND

**** INSTITUTE OF METALLURGY AND MATERIALS SCIENCE PAS, CRACOW, POLAND

GDC to the cathode. Performance of cell based on YSZ electrolyte were improved by addition of silver to LSCF cathode material [14-16].

The other way of improving cathode performance is imposing a short time external polarization. Jiang et al [25] found that even a short cathodic polarization lead to significant decrease in the Sr-doped lanthanum manganite (LSM) electrode impedance. However, in the case of noble metals the polarization can lead to metal movement along the electrolyte surface. Tens hours of negative polarization could lead to the growth of a metal deposit around a place where electrode stayed in contact with an electrolyte. Nielsen and Jacobsen found rings around platinum point electrodes being in the contact with an YSZ electrolyte after 24 h of the polarization [26-27] or silver dendrites on an YSZ electrolyte after 24 hours of the polarization [4].

The present work focuses on the improvement of the LSCF|SDC|Ni cell by addition of metallic silver to the porous LSCF cathode and describes the consequences of a short time negative and positive polarization of a silver|SDC interface.

2. Experimental

2.1. Materials preparation

20SDC was prepared from nitrates solution. The starting materials were: $\text{Ce}(\text{NO}_3)_3 \cdot 6\text{H}_2\text{O}$, $\text{Sm}(\text{NO}_3)_3 \cdot 6\text{H}_2\text{O}$ (99.9%), citric acid and ethylene glycol (99.9%, Aldrich). The reagents were mixed in distilled water in order to prepare ceria-based solid solution with the formula $\text{Ce}_{0.8}\text{Sm}_{0.2}\text{O}_{2-\delta}$. Citric acid and ethylene glycol were added to the respective nitrate solutions. The solutions were then evaporated at 70°C to obtain a hard gel, finally calcined at 900°C for 1h and then rotary-vibratory milled with a zirconia grinding media in dry ethanol. The granulated powder was cooled and isostatically pressed under 200 MPa with 5% wax-water emulsion added as a lubricant. The pellets were sintered for 2 h at 1500°C .

The samples were shaped to the form of discs of 12 and 20 mm in diameter and thickness of 0.8 mm, 1.2 mm and 2.5 mm.

LSCF was prepared also by Pechinni method. The citric acid and the ethylene glycol were added to the respective nitrate solution. The solution were also evaporated at 70°C to obtain a hard gel. The black gel was slowly heated at 500°C for 1h to remove gaseous reactants. The sample was homogenized after the heating, and finally heated at 1000°C for 1h.

The wires 0.5 mm and 1.0 mm in diameter made of silver and platinum 99.99% was supplied by Mennnica Polska S.A.

2.2. Solid oxide fuel cell preparation

The 20 SDC sintered samples were tested as oxide membranes in a two-chamber solid oxide fuel cell. An anode (50 wt%. NiO-GDC) powder (supplied by Fuel Cell Materials, USA) was mixed with terpineol and ethyl cellulose to form a slurry, subsequently screen-printed on the 20SDC electrolyte as an anode, which was heated at 1200°C for 1h. The LSCF powder was ground in a rotary-vibratory mill in dry ethylene alcohol using zirconia-grinding media. The ground LSCF powder was mixed with terpineol and ethyl cellulose to form

an ink. The ink was screen-printed through a 100-mesh silk screen onto the SDC surface and was first heated at 400°C for 2h to remove organic binders and then heated at 950°C for 12h with a heating and cooling rate of $2^\circ/\text{min}$. For the modification of the LSCF cathode with silver, a method of the nitrate decomposition was applied. In general an AgNO_3 solution with a concentration of $0.05 \text{ mol} \cdot \text{dm}^{-3}$ was dropped using a suction pipette with an accuracy of 0.01 ml and soaked into the porous LSCF cathode layer placed on the heated over hotplate to evaporate water, following by firing at 800°C for 6h.

The family of current-voltage (ΔE -I) and current-power (I-P) curves of tested solid oxide fuel cells were measured by the cyclic voltammetry (CV) method using an Autolab electrochemical station

2.3. Methods

The phase composition of all powders and sintered samples was identified by X-ray diffraction (XRD) analysis basing on the ICDD data base. XRD measurements were performed using the Panalytical X'Pert Pro system with monochromatic Cu K_α radiation. The microstructure observations were carried out using scanning electron microscope (SEM) at accelerating voltage of 20 kV equipped with back scattered electron (BSE) detector (NOVA NANO SEM 200 and E-SEM XL30, FEI). Information about the chemical composition was collected with the EDAX Genesis 4000 Energy Dispersive X-ray (EDX) spectrometer attached to the SEM.

2.4. Chronoamperometric (CA) experiments

The three electrode setup presented in Fig. 1 was used. The silver wire of the diameter 1 mm in a shape of a flat spiral was used as a counter electrode. Two silver wires of the diameter 0.5 mm folded in the shape imposed by the alumina ingot were used as a working and reference electrodes. All three silver electrodes contacted a SDC electrolyte disk were pressed by a spring located in the cold space joining the cell together. The alumina test fixture was described in a previous work [4] (Fig. 1). The experiments were performed in the stagnant air. The electrodes were connected to Gamry 300 series potentiostat/galvanostat/2RA.

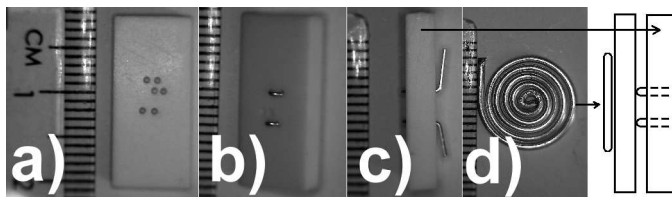


Fig. 1. The experimental setup, a – an empty alumina ingot, b and c – an ingot with mounted silver working and reference electrodes, d – a silver counter electrode. On the right side a connection of electrodes with an electrolyte is presented

2.5. Electrochemical Impedance Spectroscopy (EIS) measurements

The EIS measurements were performed using the same potentiostat, electrode setup, atmosphere and temperature. The frequency range used in the EIS measurements was from 0.1 to 300000 Hz. The amplitude of the sinusoidal voltage signal was 5 mV.

The sequence of electrochemical experiments were as follows: couple EIS spectra recordings to ensure the stability of the electrode impedance, 10 minutes of CA experiment, several EIS recordings, 10 minutes of CA experiment, several EIS recordings, 60 minutes of CA experiment performed at 600°C – during first 10 min then with cooling down the furnace. The final temperature of the cell during polarization was 350°C.

3. Results and discussion

3.1. XRD

The XRD analysis evaluated that application of Pechini method allowed us to obtain a monophase 20SDC oxide electrolyte and LSCF cathode material [28]. The 20SDC samples exhibited more than 98% of theoretical density. The typical microstructure of 20SDC sample is presented in Fig. 2. As it can be seen, 20SDC sintered sample at 1500°C-2h exhibited grain sizes in the range of 1.4 to 3.2 μm .

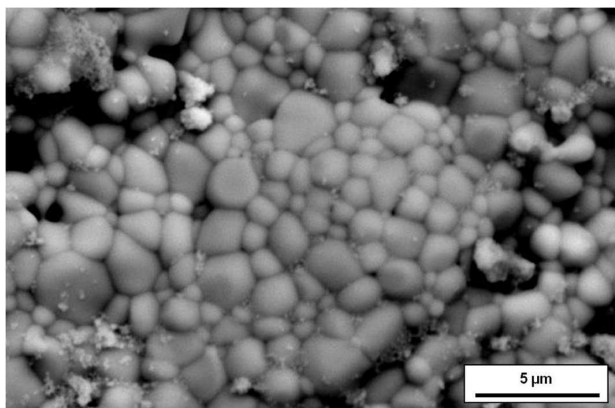


Fig. 2. Scanning electron microscopy image of the microstructure of 20SDC sintered samples prepared at 1500°C for 2 hours

3.2. Chronoamperometric experiments

The current grew up in all CA experiments performed under cathodic polarization (Fig. 3.). The current growth was continuous and can be divided into two stages. During the first one which lasted about 100 s the current grew fast, while during the second it also grew but much slower. The reason for current changes is the growth of the silver deposit visible in Fig. 3. In three consecutive experiments the recorded negative current was greater and greater although during the time between the measurements electrode partially come back to the initial state because each next CA experiment started at lower current than the previous has ended.

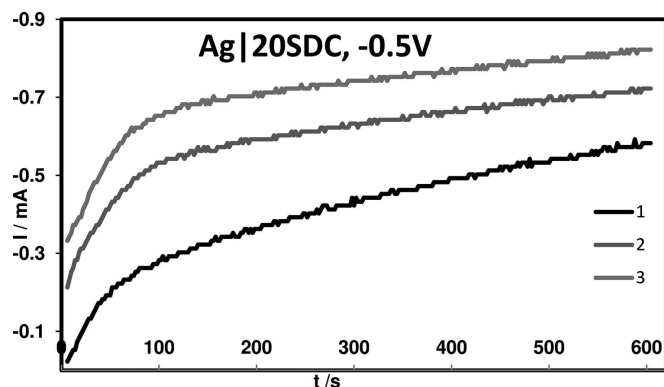


Fig. 3. Current recorded during chronoamperometric experiment on -0.5V polarized Ag|SDC interface, numbers refer to number of CA recording

The similar experiment with value of 0.5V positive polarization was performed. The growth of a current is also visible in Fig. 4. mostly at the first 100 seconds of polarization. The current grew up no more than twice. There are no periods when continuous growth of current was recorded and rather periodic deviations from the mean value are visible with couple abrupt rises. All three consecutive curves are more or less overlapping. Most of the changes occurred in the starting period of the first polarization experiment.

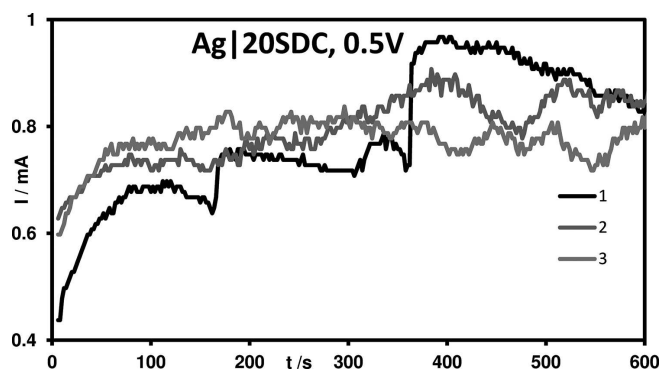


Fig. 4. Current recorded during chronoamperometric experiments on 0.5V polarized Ag|SDC interface, numbers refer to number of CA recording

3.3. EIS experiments

The EIS spectra recorded before and between CA experiments are presented in Fig. 5. The whole impedance spectrum can be divided into two or three capacitive arcs. Each arc can represent a rate-limiting step. The first high frequency (HF) arc ascribed to the electrolyte impedance is not visible or only a few points are visible on the diagrams. Arcs in the medium and low frequency range represent the electrode reaction impedance. There are two or one distinguishable arc in this frequency region. Two equivalent electrical circuits (EEC's) applied for the interpretation of spectra are presented in Fig. 6. CPE in that EEC's means the constant phase element which impedance is expressed by the following formula:

$$Z_{CPE} = \frac{1}{C_0 2\pi f_0} \left(\frac{f_0}{f} j \right)^{-\alpha} \quad (1)$$

In that formula j is the imaginary unit, f is the frequency, f_0 is the frequency of reference (in our case assumed 1000 Hz)

and C_0 is the capacitance at the frequency of reference. Each R_i CPE_i pair describes one rate determining process wherein R_1 CPE_1 is described to the electrolyte resistance and capacitance, respectively. The EEC – b was used only for fitting spectra where three distinguishable arcs are visible.

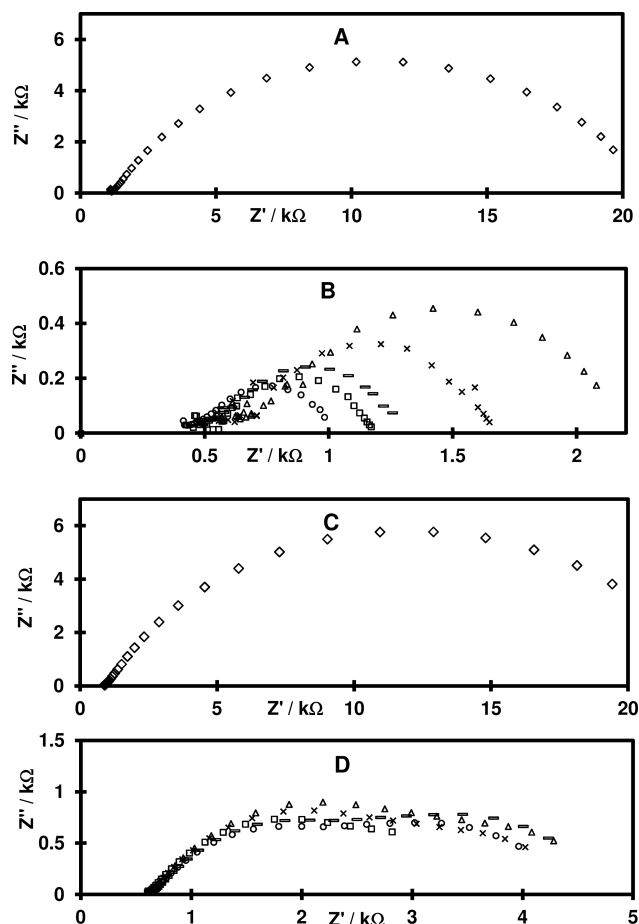


Fig. 5. Nyquist plots of the electrochemical impedance response of the silver electrodes on SDC electrolyte a) electrode before polarization used in the negative polarization experiment; b) after negative polarization: \square – 1.5 min. after the first CV experiment, \times 6 min. after the first CV experiment, Δ 12 min. after the first CV experiment, \diamond 1.5 min. after the second CV experiment, – 5 min. after the second CV experiment, c) electrode before polarization used in the positive polarization experiment; d) after positive polarization: \square – 1.5 min. after the first CV experiment, \times 7 min. after the first CV experiment, Δ – 20 min. after the first CV experiment, \diamond 1.5 min. after the second CV experiment, – 4.5 min. after the second CV experiment

The polarization resistance may be calculated from the formulae:

$$R_p = \lim_{\omega \rightarrow 0} Z = R_1 + R_2 \quad (2)$$

$$R_p = \lim_{\omega \rightarrow 0} Z = R_1 + R_2 + R_3 \quad (3)$$

for EEC – a and EEC – b, respectively. The example of fitting results are collected in TABLE 1.

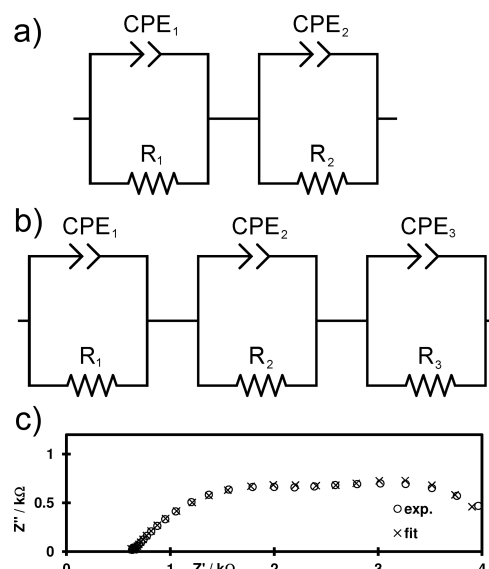


Fig. 6. Equivalent electrical circuits (EEC) used for the numerical fitting of the EIS data. CPE_1 and R_1 represent the electrolyte impedance, CPE_2 , R_2 , CPE_3 and R_3 represent the rate determining step(s) of the ORR, a) EEC for the spectra where two separate processes are visible; b) EEC for spectra where three processes are visible c) an example of fitting results

TABLE 1
Electrolyte resistance R_1 and polarization resistance R_{pol} of silver electrode obtained by fitting impedance spectra and calculated from formulae (2) or (3), respectively

Description	R_1 / Ω	R_{pol} / Ω
Before -0.5V CA experiment	1160	20900
1.5 min after 1 st 0.5V CA exp.	526	1220
7 min after 1 st 0.5V CA exp.	617	1680
10 min after 1 st 0.5V CA exp.	659	1930
13 min after 1 st 0.5V CA exp.	681	2280
1.5 min after 2 nd 0.5V CA exp.	458	1050
5 min after 2 nd 0.5V CA exp.	517	1330
Before 0.5V CA experiment	913	22800
1.5 min after 1 st 0.5V CA exp.	608	3400
4.5 min after 1 st 0.5V CA exp.	615	3560
6.5 min after 1 st 0.5V CA exp.	624	4290
10.5 min after 1 st 0.5V CA exp.	625	4440
14.5 min after 1 st 0.5V CA exp.	622	5100
19.5 min after 1 st 0.5V CA exp.	610	4940
1.5 min after 2 nd 0.5V CA exp.	643	4180
5 min after 2 nd 0.5V CA exp.	641	4520
10.5 min after 2 nd 0.5V CA exp.	644	4910

The first negative polarization CA experiment caused the decrease of polarization resistance by 16 times and electrolyte resistance by 2 times whereas positive one caused by 5 times decrease of polarization resistance and 50% decrease of electrolyte resistance.

Both discussed resistances of the negatively polarized electrode increased during the time between CA experiments in similar manner. The reason of these changes can be attributed to the modification of the contact area and the length of the tpb line.

In the case of positively polarized electrode between CA experiments, the polarization resistance grew up much slower whereas the electrolyte resistance remained stable. The shape of the impedance spectra changed after CA experiments. Three semicircles are visible in the Fig. 5d.

3.4. Structural and microstructural changes

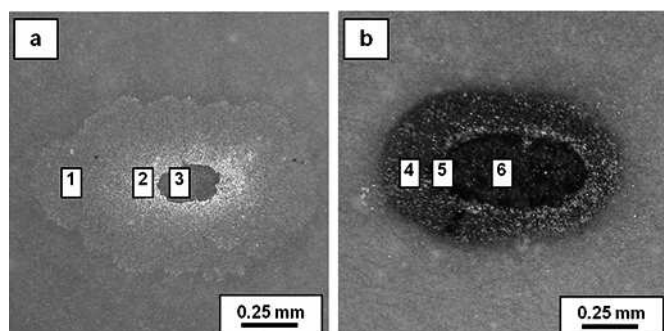


Fig. 7. The optical microscope image of the SDC electrolyte surface after EIS and CA experiments: -0.5 V (a) polarized electrode and 0.5 V one (b). Numbers 1-6 denotes the areas of further SEM investigation presented in Fig. 8

Observation of an electrode surface under optical microscope after negative polarization experiments revealed a silver color ellipse with 1.3 mm long major axis around the point where the electrode stayed in contact with the electrolyte

(Fig. 7a). A small hole in the center was of the same shape as the piece of SDC left on the silver electrode. On the other hand, after positive polarization experiments the visual observation of an electrode surface showed the presence of a black ellipse with 1.3 mm long major axis around the point where the electrode was contacted the electrolyte (Fig. 7b). A clear difference between the both cases – especially the black color of the surface after positive polarization experiment, was the reason for further SEM examination. Figure 8 represents three characteristic areas of the electrode surface after negative (in Fig. 8 No.1-3) and positive polarization (in Fig. 8 No.4-6) which can be described as external part of ellipse (Fig. 8: 1,4), internal part (Fig. 8: 3,6) and their border (Fig. 8 No: 2,5). The SEM examination of the surface subjected to the negative polarization showed the presence of a lot of metallic silver which took different shape depending on the location. Within the external area (Fig. 8-1) rather separated balls of Ag were visible. In contrary to this the area of the border between the external and internal part (Fig. 8-2) was decorated by the metallic silver in a form of connected short wires creating a flat net around the point of electrode-electrolyte contact. That deposit enlarged this contact area as well as a tpb length as it was described by Mosiałek et al [4]. Any presence of silver was detected within the internal area presented in Fig. 8-3.

On the other hand, the external area of the surface after positive polarization experiment visible in Fig. 8-4 demonstrated the presence of both metallic silver in the shape of balls and silver oxide responsible for the black color. Furthermore, the border area (Fig. 8-5) was composed of solely silver oxide taking shapes of flakes with large number of nanosized pores. Similarly to this, the internal part (Fig. 8-6) consisted also of the silver oxide and only exceptional presence of metallic silver was detected (see arrow).

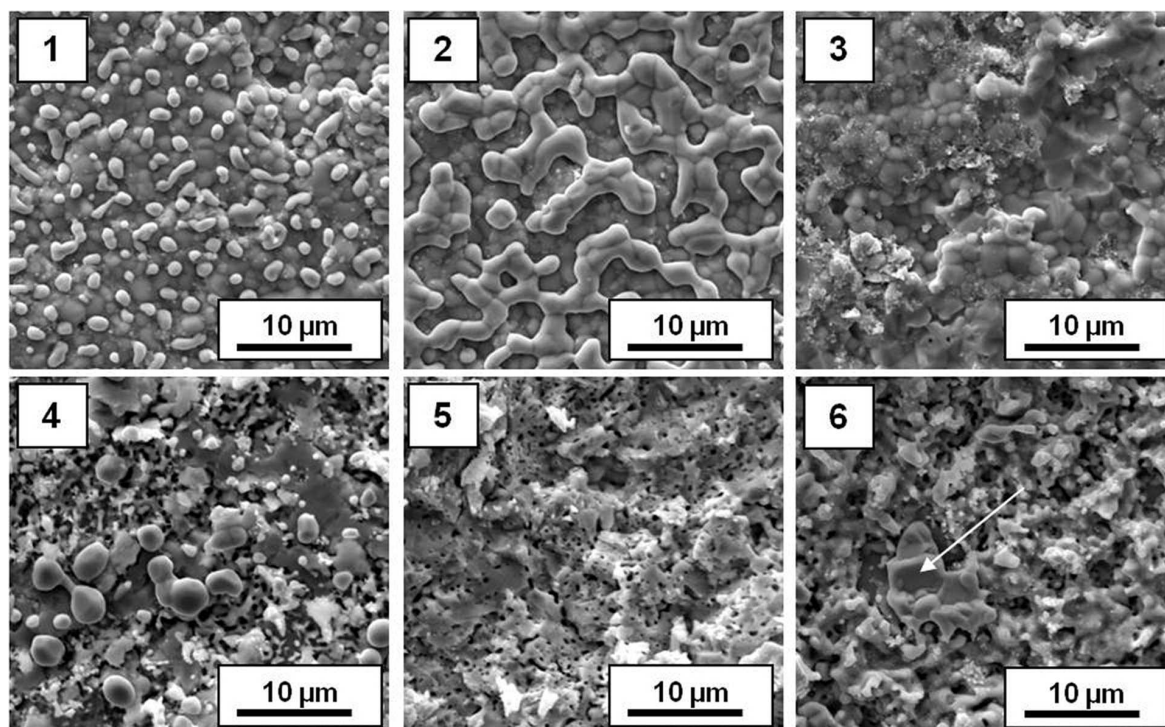


Fig. 8. SEM (SE) images of 20SDC surface microstructure near the border of the areas marked with No. 1-6 in Fig. 7, where silver electrode was in contact with the electrolyte after - 0.5 V polarization (1-3), after 0.5 V polarization (4-6)

3.5. Composite cathode Ag/LSCF

The idea of improving the power and current densities acquired from an IT-SOFC with 20SDC electrolyte could be through the utilization of Ag/LSCF as a composite cathode. Fig. 9. presents the SEM microphotograph of the Ag/LSCF composite cathode. As it can be seen, the Ag/LSCF cathode is porous, and Ag particles of sizes in the range 0.4 to 2 μm are randomly distributed on the surface of LSCF of cathode materials. Fig. 10. presents the family of curves (ΔE -I and P-I) recorded for the IT-SOFC with a 20SDC electrolyte and a LSCF or Ag/LSCF cathode at 700°C. As it can be observed that there is an increase of a power and a current density for the IT-SOFC with 20SDC electrolyte and with a Ag/LSCF composite cathode compared to the similar IT-SOFC containing only the monophasic LSCF cathode material.

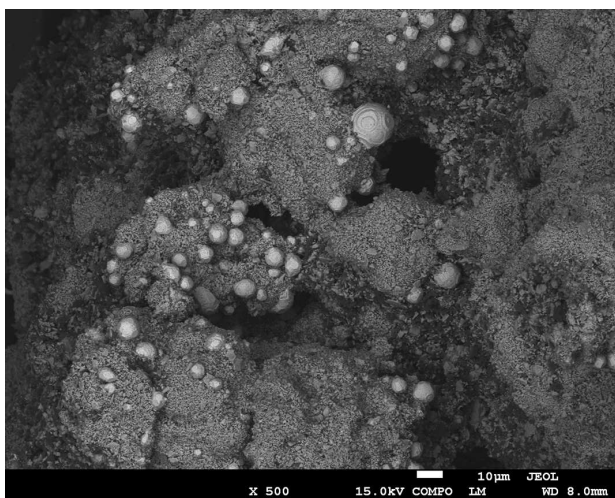


Fig. 9. SEM microphotograph of the Ag/LSCF composite cathode

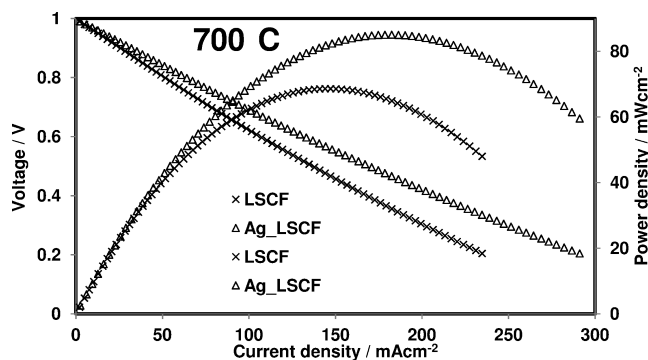


Fig. 10. The family of P-I curves recorded for IT-SOFC with a 20SDC solid electrolyte with monophasic cathode LSCF or LSCF+5% wt. Ag at 700°C

4. Conclusions

The short time polarization of silver or silver containing electrodes contacted with SDC electrolyte can cause noticeable decrease of the electrode impedance. This decrease was observed after both negative and positive polarizations. The 100 second is enough time to made almost the whole activation. During the polarization process the noticeable silver

position rearrangement in the electrode structure takes place. Positive polarization gives more stable decrease of the electrode impedance.

The addition of metallic silver to LSCF electrode improve the electrode performance by 33% in LSCF|SDC|Ni fuel cell.

Acknowledgements

This work was financially supported by Polish Ministry of Science and Higher Education (grant No 6166/B/T02/2010/38).

The part of the experiment concerning SEM/EDS measurements of SDC were performed within Accredited Testing Laboratories at the Institute of Metallurgy and Materials Science of the Polish Academy of Sciences.

REFERENCES

- [1] R. Baker, J. Guindet, M. Kleitz, J. Electrochem. Soc. **144**, 2427 (1997).
- [2] R. Jiménez, T. Kloidt, M. Kleitz, J. Electrochem. Soc **144**, 582 (1997).
- [3] P.S. Ho, H.B. Huntington, Journal of Physics and Chemistry of Solids **27**, 1319 (1966).
- [4] M. Mosiałek, E. Bielańska, R.P. Socha, M. Dudek, G. Mordarski, P. Nowak, J. Barbasz, A. Rapacz-Kmita, Solid State Ionics **225**, 755 (2012).
- [5] A. Jaiswal, E. Wachsmann, Solid State Ionics, **177**, 677 (2006).
- [6] M. Camaratta, E. Wachsmann, Solid State Ionics **178**, 1242 (2007).
- [7] M. Camaratta, E. Wachsmann, Solid State Ionics **178**, 1411 (2007).
- [8] C. Xia, Y. Zhang, M. Liu, Appl. Phys. Lett **82**, 901 (2003).
- [9] K. Sasaki, K. Hosoda, T.N. Lan, K. Yasumoto, S. Wang, M. Dokiya, Solid State Ionics **174**, 97 (2004).
- [10] V. Haanappel, D. Rutenbeck, A. Mai, S. Uhlenbruck, D. Sebold, H. Wesemeyer, B. Röwekamp, C. Tropartz, F. Tietz, J. Power Sources **130**, 119 (2004).
- [11] S. Uhlenbruck, F. Tietz, V. Haanappel, D. Sebold, H.-P. Buchkremer, S. Detlev, J. Solid State Electrochem. **8**, 923 (2004).
- [12] W. Zhou, R. Ran, Z.P. Shao, R. Cai, W.Q. Jin, N.P. Xu, J. Ahn, Electrochim. Acta **53**, 4370 (2008).
- [13] Z. Gao, Z. Mao, J. Huang, R. Gao, C. Wang, Z. Liu, Mater. Chem. Phys. **108**, 290 (2008).
- [14] S.P. Simner, M.D. Anderson, J.E. Coleman, J.W. Stevenson, J. Power Sources **161**, 115 (2006).
- [15] Y. Sakito, A. Hirano, N. Imanishi, Y. Takeda, O. Yamamoto, Y. Liu, J. Power Sources **182**, 476 (2008).
- [16] K. Murata, A. Hirano, N. Imanishi, Y. Takeda, ECS Transactions **25**, 2413 (2009).
- [17] M. Dudek, M. Mosiałek, G. Mordarski, R.P. Socha, A. Rapacz-Kmita, Archives of Metallurgy **56**, 1249 (2011).
- [18] Q. Li, L.-P. Sun, L.-H. Huo, H. Zhao, J.-C. Grenier, J. Power Sources **196**, 1712 (2011).
- [19] S. Huang, Z. Zong, C. Peng, J. Power Sources **173**, 415 (2007).
- [20] S.B. Adler, J. Electrochem. Soc. **143**, (1996).
- [21] V. Dusastre, J.A. Kilner, Solid State Ionics **126**, 163 (1999).
- [22] J.W. Fergus, J. Power Sources **189**, 30 (2006).

- [23] S. Pinol, M. Morale, F. Espirell, J. Power Sources **169**, 2 (2007).
- [24] M. Dudek, A. Rapacz-Kmita, M. Mroczkowska, M. Mosiałek, G. Mordarski, Electrochim. Acta **55**, 4387 (2010).
- [25] S.P. Jiang, J.G. Love, J.P. Zhang, M. Hoang, Y. Ramprakash, A.E. Hughes, S.P.S. Badwal, Solid State Ionics **121**, 1 (1999).
- [26] J. Nielsen, T. Jacobsen, Solid State Ionics **178**, 1001 (2007).
- [27] J. Nielsen, T. Jacobsen, Solid State Ionics **178**, 1769 (2008).
- [28] M. Dudek, Journal of the European Ceramic Society **28**, 965 (2008).

Received: 10 September 2012.